Title

Displacement-Based Design of Axially Loaded Piles for Seismic Loading and Liquefaction-Induced Downdrag

Journal

Journal of Geotechnical and Geoenvironmental Engineering, 149(9)

ISSN

1090-0241

Authors

Sinha, Sumeet K
Ziotopoulou, Katerina
Kutter, Bruce L

Publication Date

2023-09-01

DOI

10.1061/jggefk.gteng-11178

Peer reviewed

Displacement-Based Design of Axially Loaded Piles for Seismic Loading and Liquefaction-Induced Downdrag

Sumeet K. Sinha, A.M.ASCE[1]; Katerina Ziotopoulou, M.ASCE[2]; and Bruce L. Kutter, M.ASCE[3]

Abstract: Axially loaded piles in liquefiable soils can undergo severe settlements due to a shaking event. During shaking, the settlement is caused by the reduction of its shaft and tip capacity from the excess pore pressures generated around the pile. Post shaking, additional pile settlement is caused by the surrounding soil settling due to reconsolidation and the associated development of drag load. A new displacement-based method is developed using a TzQzLiq analysis for designing axially loaded piles subject to seismic loading and liquefaction-induced downdrag. The new displacement-based design method offers several advancements to the state of practice forced-based design procedure by AASHTO's force-based design procedure by reasonably accounting for the mechanisms that occur on axially loaded piles during and post shaking. It accounts for the initial drag load on the pile, redistribution effects resulting in large excess pore pressures in the non-liquefied layers, and reduction in the pile's shaft and tip capacity from excess pore pressures around the pile. The new design procedure estimates the pile settlement and axial load distribution during the entire shaking event, i.e., during shaking and reconsolidation. Design steps are provided describing the procedure for obtaining design curves on the settlement and drag load on piles with varying pile lengths. The length of the piles is then selected based on serviceability criteria and the pile's structural strength. Finally, the new design procedure is applied on piles used in centrifuge model tests, and results are compared, followed by an example design problem that illustrates the applicability of the new method in practice. **DOI: 10.1061/JGGEFK.GTENG-11178.**

Author keywords: Pile design; Liquefaction; Seismic loading; Downdrag; Axial load.

Introduction

Axially loaded piles in liquefiable soils can undergo severe settlements due to shaking. During shaking, the settlement is caused by the loss of shaft and tip resistance from the generated excess pore pressures (u_e) in the soil and seismic loads on the pile. After shaking, soil settlement from reconsolidation results in the development of a drag load leading to the additional settlement of the pile. Madabhushi et al. (2010) and Kaynia (2022) describe the mechanisms affecting the response of axially loaded piles in liquefiable soils, which are also illustrated in Fig. 1. Generally, a pile resists the dead load (Q_{dead}) (from the superstructure) by mobilizing positive skin friction (positive shaft resistance) and tip resistance [Fig. 1(a)]. During shaking, u_e generation around the pile reduces the positive skin friction in that layer, transferring load further down the shaft and to the tip. Moreover, the shaking of the superstructure induces a cyclic seismic load (Q_{seismic}) on the pile [Fig. 1(b)]. The pile resists the seismic load with the reduced shaft and tip capacity by undergoing settlement until enough resistance is mobilized to achieve force equilibrium. When u_e develop around the pile's tip, the tip capacity and stiffness are reduced, potentially causing more settlement in a pile. The loss of the confinement around the pile from increased u_e may also buckle the pile (Bhattacharya et al. 2004). At the end of shaking, $Q_{\text{seismic}} = 0$, and only the dead load acts on the pile [Fig. 1(c)]. However, post shaking, soil settlement due to reconsolidation ensues and causes downdrag, resulting in drag loads (from negative skin friction) on the pile [Fig. 1(c)]. Consequently, the decrease in u_e from reconsolidation also increases tip capacity. The depth at which the soil and the pile settle equally (i.e., their relative movement is zero) is known as the neutral plane (Fellenius 1984). At this depth, the skin friction changes its direction from negative to positive. Above the neutral plane, the soil settles more than the pile resulting in negative skin friction [Figs. 1(c and e)]. Below the neutral plane, the pile settles more than the soil resulting in positive skin friction [Figs. 1(c and e)]. The drag load increases the load on the pile and decreases the length of the portion of the pile, providing positive skin friction. As a result, more load is transferred to the shaft and tip below the neutral plane, and the pile settles [Figs. 1(c and d)]. After complete reconsolidation, a permanent drag load (Q_{drag}) may remain, and the neutral plane moves deeper into the liquefiable layer [Figs. 1(d and e)]. Due to drag load, the distribution of axial load along the pile increases from its head toward the neutral plane, maximizes at the neutral plane (Q_{np}) and decreases below that [Fig. 1(f)].

Existing procedures for designing piles in liquefiable soils do not fully account for the mechanisms observed during shaking and reconsolidation. The state of practice, AASHTO (2020), uses a forced-based approach to design piles in liquefiable soils. First, the total load acting on the pile is statically checked against the total available resistance with appropriate load and resistance factors for service and strength limit design. Then, for extreme loading conditions (e.g., seismic loads during shaking and liquefaction-induced downdrag), the superstructure's integrity is checked against the

[1]Assistant Professor, Dept. of Civil Engineering, Indian Institute of Technology Delhi, New Delhi 110016, India (corresponding author). ORCID: https://orcid.org/0000-0002-2011-4887. Email: sksinha@civil.iitd.ac.in

[2]Associate Professor, Dept. of Civil and Environmental Engineering, Univ. of California Davis, One Shields Ave., Davis, CA 95616. ORCID: https://orcid.org/0000-0001-5494-497X. Email: kziotopoulou@ucdavis.edu

[3]Professor Emeritus, Dept. of Civil and Environmental Engineering, Univ. of California Davis, One Shields Ave., Davis, CA 95616. ORCID: https://orcid.org/0000-0002-0628-1275. Email: blkutter@ucdavis.edu

Note. This manuscript was submitted on July 12, 2022; approved on April 26, 2023; published online on July 7, 2023. Discussion period open until December 7, 2023; separate discussions must be submitted for individual papers. This paper is part of the ***Journal of Geotechnical and Geoenvironmental Engineering***, © ASCE, ISSN 1090-0241.

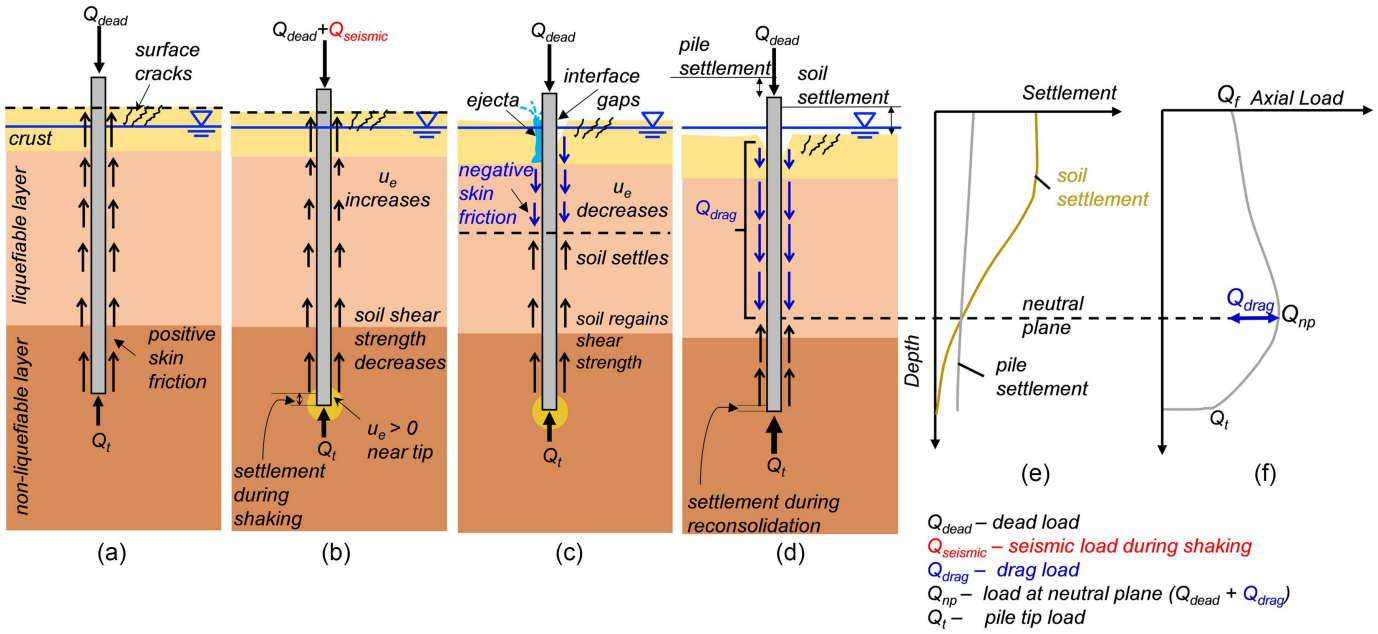

Fig. 1. Illustration of mechanisms affecting the axial response of piles in liquefiable soils: (a) distribution of positive skin friction and tip resistance in a pile before shaking; (b) loss of shaft and tip capacity due to generated excess pore pressures (u_e), development of seismic loads, and resulting pile settlement during shaking; (c) dissipation of excess pore pressures (u_e) and development of negative skin friction due to soil reconsolidation; (d) developed drag load, final depth of the neutral plane; (e) soil and pile settlement; and (f) distribution of axial load along a pile after complete reconsolidation.

updated pile's total capacity and structural strength: for the pile's capacity during shaking, the shaft capacity in the liquefied ($r_u = 1$) layer is assumed zero while assuming total shaft and tip capacity in the non-liquefied layers ($r_u < 1$). AASHTO (2020) does not recommend evaluating reduced shaft or tip capacities in non-liquefied layers, essentially ignoring any effect of excess pore pressure generation or redistribution from the liquefied layers. However, recent studies on axially loaded piles in liquefiable soils (e.g., Knappett and Madabhushi 2009; Sinha et al. 2022a, b, c, 2023) showed that estimating u_e and their effect on reducing the pile's capacity is crucial for pile design. Knappett and Madabhushi (2009) found that the pile tip capacity and stiffness decreased as the u_e increased around the pile's tip, and respectively increased as u_e decreased during reconsolidation. After complete reconsolidation, the tip capacity can either be fully regained or even higher than its initial value if the pile suffers significant settlement. Stringer and Madabhushi (2013a, b) conducted several centrifuge tests and found that the presence of an impermeable overlying soil layer, the redistribution of u_e from the loose liquefied layer can increase u_e in the dense sand (bearing) layer. In this scenario, piles suffer substantial settlements during shaking (when u_e increased near the pile's tip) compared to during reconsolidation (when u_e decreased). Conversely, the presence of a highly permeable overlying soil layer facilitates a more rapid reconsolidation and, therefore, smaller u_e in the dense sand layer and a faster regain of tip capacity resulting in an overall smaller pile settlement. Sinha et al. (2021b) conducted centrifuge model tests on three identical axially loaded piles embedded three diameters into a dense sand layer with small, medium, and large pile head loads (Q_f), resulting in a static factor of safety of 8, 2.6, and 1.6, respectively. Through these tests, Ziotopoulou et al. (2022) and Sinha et al. (2022a) found that most of the pile settlement occurred during shaking when high u_e in the soil surrounding the pile reduced its shaft and tip capacity. In these tests, Sinha et al. (2023) observed significant u_e generation in the dense sand (bearing) layer due to the redistribution of u_e from the adjacent liquefied layer (Seed et al. 1976; Yoshimi and Kuwabara 1973). The high u_e developed near the pile's tip caused large settlements of the piles. Across multiple shaking events, the settlement of the pile increased as the u_e near the tip increased (Fig. 2), ultimately leading to the piles with medium and large head loads plunging into the soil (Fig. 2). Stringer and Madabhushi (2013b) conducted centrifuge tests on free-standing and cap-supported pile groups. They found that during plunging failure, the pile cap provided additional resistance, thus limiting the overall settlement of the piles. Particularly for accounting for the liquefaction-induced downdrag in pile design, AASHTO (2020) recommends considering the neutral plane at the bottom of the deepest liquefied layer or at the depth where soil settlement equals 10 mm. The drag load is then calculated as the total negative skin friction above the neutral plane. AASHTO (2020) "conservatively" assumes the negative skin friction is equal to the "residual shear strength" in the reconsolidated

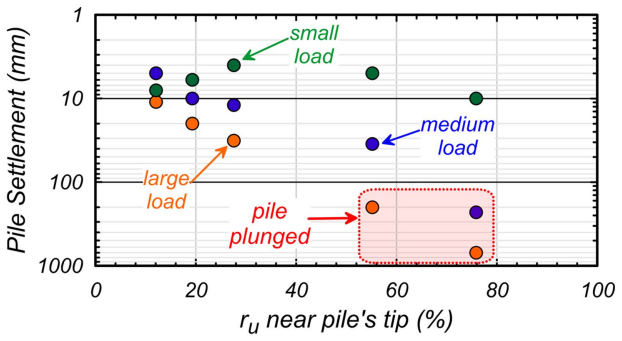

Fig. 2. Effect of excess pore pressure ratio (r_u) near the pile's tip on settlement of three identical piles embedded at the same depth with small, medium, and large pile head loads, resulting in a static factor of safety of 8, 2.6, and 1.6, respectively. (Data from Ziotopoulou et al. 2022.)

J. Geotech. Geoenviron. Eng., 2023, 149(9): 04023076

liquefied soil and non-liquefied shear strength (i.e., equal to the soil shear strength) in the non-liquefied soil. The factored drag load (Q_{drag}) is then added to the factored pile head load (Q_{dead}) and checked against the total resistance provided by the pile length below the neutral plane [Figs. 1(d and f)], ignoring any pile movement. However, contrary to the force-based method, if the pile settles relative to the soil, the negative skin friction will change to positive skin friction, providing resistance to the pile. AASHTO (2020) also does not recognize the presence of initial (i.e., before shaking) drag load in the piles and its effect on the downdrag phenomenon. Furthermore, AASHTO (2020) does not provide a method for calculating the pile's settlement; hence, it cannot be used for displacement-based design.

A displacement-based design approach offers the advantage of directly evaluating the performance of piles in terms of their settlement. The centrifuge studies by Sinha et al. (2021a, b) and Stringer and Madabhushi (2013a, b) have confirmed that the resulting pile settlement is small even while large drag loads are caused by liquefaction-induced downdrag. Among various methods, a displacement-based approach using t-z and q-z springs analyses may be used to estimate the load distribution and settlement of piles. The t-z material models the behavior of shaft resistance, and the q-z material models the tip resistance. Law and Wilson (2017) used a displacement-based design procedure using t-z and q-z materials and reduced pile length by 20% compared to the force-based design procedure from AASHTO (2020). Boulanger et al. (1999) developed a TzLiq material to account for shaft resistance and stiffness changes as excess pore pressures developed and dissipated in the soil around the pile. That TzLiq material modeled capacity and stiffness as a linear function of u_e in the adjacent soil. Boulanger and Brandenberg (2004) used the TzLiq material to model liquefaction-induced downdrag on axially loaded piles accounting for u_e dissipation with the associated soil settlement. Kim and Mission (2011), Wang and Brandenberg (2013), and Wang et al. (2015) used a TzLiq material to compute consolidation-induced drag load and downdrag settlement in clay. The model assumed a constant mobilization of tip load equal to the undrained tip resistance. Wang et al. (2015) modeled the pile's tip resistance to vary nonlinearly (based on pile settlement) between the undrained tip resistance existing before the earthquake and after complete reconsolidation. Lam et al. (2009) and Sun and Yan (2010) used three-dimensional (3D) axisymmetric finite element analyses to investigate drag load and settlement of piles in consolidating clay layers with rigid tip conditions. Sinha et al. (2022c) developed a QzLiq material to model tip behavior in liquefiable soils. The pile's tip capacity and stiffness were varied nonlinearly, with u_e at the tip i.e., $(1 - r_u)^{\alpha_t}$, where α_t is a constant defined by Knappett and Madabhushi (2009) that is a function of the soil's friction angle (ϕ). Sinha et al. (2022c) used the TzLiq and the QzLiq material and performed a TzQzLiq analysis to model the response of axially loaded piles in liquefiable soils and validated the numerical results against centrifuge test data. The numerical model accounted for the initial drag load on piles, changes in the shaft and tip capacities and stiffnesses in the presence of u_e in soil, and the timing of soil settlement and u_e distribution. The TzQzLiq analysis yielded time histories of axial load distribution and settlement of piles during and after shaking.

This paper presents a displacement-based design procedure for single piles, such as monopile foundations used in offshore wind farms for energy generation, transmission line foundations, and large diameter drilled piers. It uses the TzQzLiq analysis methodology for designing axially loaded piles subject to seismic loading and liquefaction-induced downdrag. The procedure accounts for the initial drag load on the pile, excess pore pressures in the non-liquefied layers following redistribution from the liquefied layers, and reduction in the pile's shaft and tip capacity from excess pore pressures in the soil profile. However, the proposed procedure does not account for the pile cap effects, which may provide additional resistance and limit the settlement of the pile during plunging failures (Stringer and Madabhushi 2013b). Design steps are provided to estimate the input properties required for running a TzQzLiq analysis. Results from the analysis are then used to obtain design curves describing the settlement and drag load on the pile with varying pile lengths, which are then ultimately used for selecting the design length of the pile. Finally, the design procedure is applied to the piles used in centrifuge tests and the results are compared. The paper concludes with an example design problem to illustrate the applicability of the new method in practice (see Appendix A) and a discussion of the results.

Displacement-Based Design Method

Extreme events considered in pile design include seismic loading and liquefaction-induced downdrag. A TzQzLiq analysis of piles (Sinha et al. 2022c) can be performed in three stages (shown in Fig. 3) to obtain the axial load distribution and settlement of piles from these loading conditions. Stage 1 applies a pile head load ($Q_f = Q_{dead}$) and simulates the initial axial load distribution on the pile. Stage 2 and Stage 3 model the extreme loading events (as described in the following subsections), respectively. Results from the TzQzLiq analysis can be used to obtain design curves on drag load and pile settlement for varying pile lengths. The pile length can then be selected based on serviceability criteria and checked against the structural strength of the pile. The serviceability criteria could be based on the total pile settlement or the differential pile settlement relative to the free-field settlement. Additionally, pile buckling instability during shaking can also be checked using the procedure described by Bhattacharya and Madabhushi (2008).

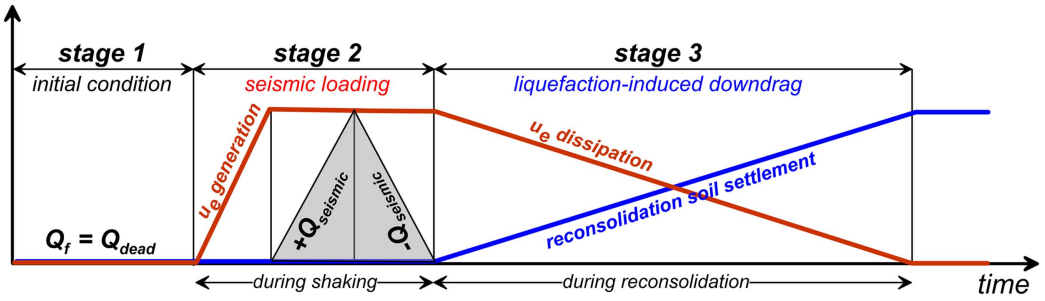

Fig. 3. Stages of modeling in the TzQzLiq analysis.

J. Geotech. Geoenviron. Eng., 2023, 149(9): 04023076

Design for Seismic Loading

During shaking, excess pore pressures in the soil around the pile may decrease its shaft and tip capacity. At the same time, the seismic shaking of the superstructure may impose cyclic loads (Q_{seismic}) on the pile, which can be estimated by analyzing the superstructure under the design earthquake load. AASHTO (2011) suggests methods for determining seismic loads on bridges and their foundations. Additionally, near-surface liquefaction leading to surface manifestation and material removal from the vicinity of the piles can cause a complete reduction of shaft resistance above the liquefied layer (Caltrans 2020).

A conservative approach for estimating the settlement of piles during shaking would be to perform a TzQzLiq analysis with a dead load of $Q_f = Q_{\text{dead}}$, followed by reducing the shaft and tip resistance due to u_e and then applying cycles of seismic load ($\pm Q_{\text{seismic}}$) to the pile head. This analysis approach is conservative as it assumes the application of seismic loads at the state when u_e is maximum in the soil around the pile. An illustration of the sequence of loads applied on the pile and the u_e in the soil while performing a TzQzLiq analysis for seismic loading is shown in Stage 2 of Fig. 3. During real earthquake shaking, the pile can experience multiple cycles of the seismic load depending on the ground motion's duration, intensity, and its predominant period relative to that of the superstructure. The pile settlement caused by seismic loading is expected to be most prominent in the first cycle with the greatest amplitude and significantly lower during subsequent and lower amplitude cycles (Wang et al. 2021). Therefore, applying one cycle of the maximum expected seismic load while the pile capacity is at its minimum is suggested (in this procedure) to provide a reasonable estimate of pile settlement for most earthquake loading conditions. However, if the superstructure experiences multiple loading cycles (e.g., in a long duration earthquake), those need to be adequately accounted for to assess pile settlement from multiple cyclic seismic loads.

Design for Liquefaction-Induced Downdrag

During reconsolidation, only the dead load acts on the pile [Figs. 1(c) and 3]. Thus, the proposed approach for estimating the pile settlement during reconsolidation is to consider a dead load ($Q_f = Q_{\text{dead}}$) acting on the pile with excess pore pressures decreasing as soil settlement occurs. An illustration of the pile load, the time history of excess pore pressures, and soil settlement considered while performing a TzQzLiq analysis for liquefaction-induced downdrag are shown in Stage 3 of Fig. 3.

TzQzLiq Material Properties

The TzQzLiq numerical model uses TzLiq and QzLiq materials [Fig. 4(e)] with zero-length elements to model the response of piles in liquefiable soils (Sinha et al. 2022c). These materials account for changes in the shaft and tip capacity of the pile as free-field excess pore pressures are generated and later dissipated [Fig. 4(e)]. The reduced shaft capacity ($t_{\text{ult}}^{r_u}$) and tip capacity ($q_{\text{ult}}^{r_u}$) are each modeled as a function of the excess pore pressure ratio (r_u) around the pile's shaft and near the tip as defined in the following equations:

$$t_{\text{ult}}^{r_u} = t_{\text{ult}}^{o}(1 - r_u)$$
$$q_{t,\text{ult}}^{r_u} = q_{t,\text{ult}}^{o}(1 - r_u)^{\alpha_t}$$
$$\alpha_t = \frac{3 - \sin\phi'}{3(1 + \sin\phi')} \quad (1)$$

where t_{ult}^{o} and $q_{t,\text{ult}}^{o}$ are the ultimate tip and shaft capacities, respectively, when $r_u = 0$. Both can be obtained empirically using equations and correlations provided in AASHTO (2020) or directly measured from the field or lab tests. The parameter α_t is a constant that, according to Knappett and Madabhushi (2009), depends only on the effective friction angle (ϕ') of the soil at the tip.

The stiffness of the TzLiq and QzLiq materials in liquefiable soils are scaled proportionally to the respective shaft ($t_{\text{ult}}^{r_u}$) and tip ($q_{\text{ult}}^{r_u}$) capacities defined in Eq. (1). Sinha et al. (2022c) describe the selection of stiffness parameter z_{50} (i.e., the displacement corresponding to 50% of ultimate capacity) for the implemented material models TzLiq and QzLiq in OpenSees (McKenna et al. 2010). The stiffness parameter of the TzLiq material can be estimated, assuming a displacement in the order of 3% of the pile diameter can mobilize the interface skin friction capacity (Sinha et al. 2022b, c). The stiffness parameter (z_{50}) can accordingly be chosen based on the backbone curve of the t-z material. For example, the nonlinear backbone curve of the implemented t-z material (Boulanger et al. 1999; Mosher 1984; Reese and O'Neil 1987) in OpenSees is a hyperbolic curve that takes a displacement equal to about four times z_{50} to mobilize >90% of t_{ult}^{o}. Thus, a z_{50} of 0.5% of the pile's diameter can be assumed for modeling the stiffness of the TzLiq material.

Determining a site-specific QzLiq material stiffness is essential for accurately modeling the pile settlement and drag load. Sensitivity studies on TzLiq and QzLiq material stiffness for axially loaded piles in liquefiable soils by Sinha et al. (2022c) found that the QzLiq stiffness significantly affected pile settlement and drag load development. Therefore, that study recommended calibrating the QzLiq material's initial capacity and stiffness against site-specific pile load tests (PLT). For the cases when a PLT is not available, an empirical PLT curve is developed to aid in the QzLiq material calibration. Well-documented PLT data from the Federal Highway Administration's (FHWA) Deep Foundation Load Test Database (DFLTD)—Version 2.0 (Petek et al. 2016) were used to develop the empirical pile load test curve. Pile load tests from large diameter (>20 in.) cast-in-drilled-hole (CIDH) piles of slenderness ratio (L/D) of about 20 were used to develop the empirical curve. Fig. 5 shows the empirical pile load test curve. It also summarizes the projects and the properties of the piles [diameter, slenderness ratio (L/D), and the bearing layer friction angle (ϕ')] used for developing it. The equation of the empirical pile load test curve is:

$$\Delta_p = a \cdot \exp(b \cdot P/P_{\Delta_p=5\%D}) - a \cdot \exp(c \cdot P/P_{\Delta_p=5\%D}) \quad (2)$$

where P = pile capacity; Δ_p = pile settlement in % of pile's diameter; $P_{\Delta_p=5\%D}$ = pile capacity corresponding to the settlement equal to 5% of the pile's diameter; and a, b, and c = constants equal to 0.24, 3.3, and 1.83, respectively. The functional form of Eq. (2) (with displacement as a function of the load) was chosen to represent the pile load test, where the load (P) is applied on the pile and settlement (Δ_p) is measured. It can be seen from Fig. 5 that the empirical pile load test curve matches quite well with the field data.

Proposed Design Procedure

Obtaining design curves relating settlement and drag load to pile length requires several steps. These have been labeled as (a–f) in the proposed design procedure and are illustrated in Fig. 4. A pile design problem includes information on soil layer properties, pile properties, design earthquake motion, design loads, and serviceability criteria (see Appendix A). The information provided in

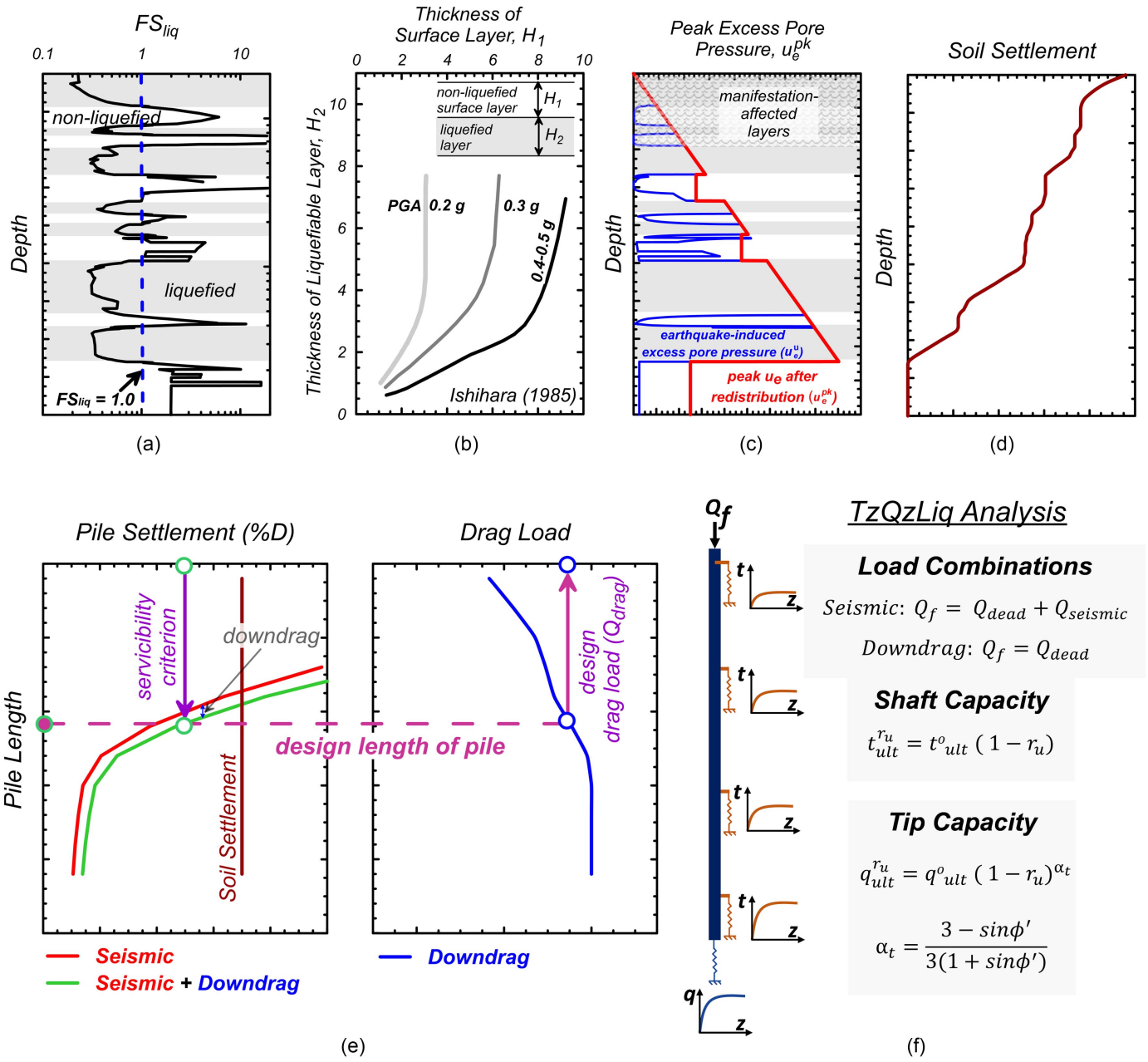

Fig. 4. Illustration of the steps involved in the proposed displacement-based design procedure: (a) liquefaction hazard analysis; (b) evaluation of surface manifestation potential (data from Ishihara 1985); (c) peak excess pore pressures estimation; (d) reconsolidation settlement estimation; (e) pile settlement estimation by running a TzQzLiq analysis; and (f) pile design curves on pile settlement and drag load for varying pile lengths.

the pile design problem was used in Steps (a) to (d) to obtain the input parameters for performing TzQzLiq analysis (Step e), whose results were then used to obtain design curves (Step f). The input parameters for a given design earthquake motion were: the factor of safety against liquefaction (FS_{Liq}) (Step a), the soil layers affected by surface manifestation (Step b), profiles of peak excess pore pressure (u_e^{pk}) (Step c), and soil settlement profile (Step d). The t-z and q-z material properties were estimated from the soil layer, pile properties, and pile load test results (if available) as described in the section "TzQzLiq Material Properties." With the obtained input parameters and t-z/q-z material properties, multiple TzQzLiq analyses (Step e) were performed to obtain design curves on pile settlement and drag load with varying pile lengths (Step f). Finally, the serviceability criteria on pile settlement and the pile's structural strength were used on the design curves to determine the design length of the pile. Appendix A demonstrates a step-by-step application of the proposed design procedure on an example problem and compares the results with Caltrans' (2020) method. The following subsections describe the design steps in detail.

Liquefaction Hazard Analysis

A liquefaction hazard analysis was performed for a given design earthquake loading to estimate the factor of safety against liquefaction (FS_{liq}) and identify the soil layers that are expected to liquefy. During shaking, the layers expected to liquefy will achieve $r_u = 1.0$ (hence referred to as "liquefied" layers), while the rest of the soil layers will result in $r_u < 1.0$ (referred to as "non-liquefied" layers). A non-liquefiable layer, such as a clay layer, can be assumed to

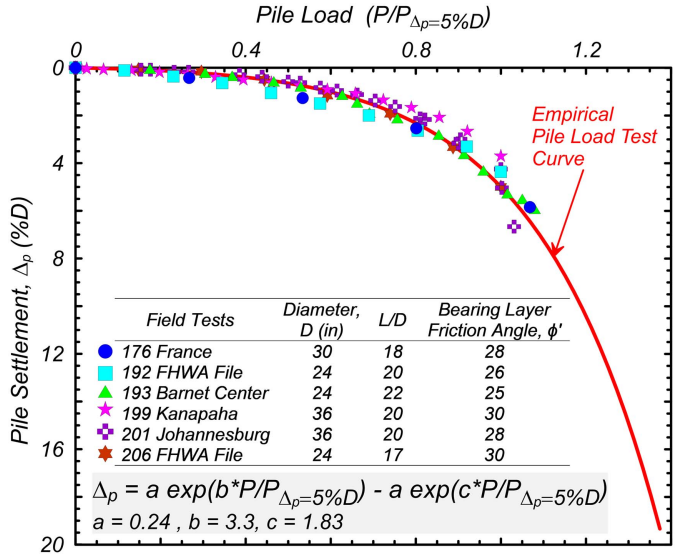

Fig. 5. Empirical pile load test curve for large diameter (>20 in.) CIDH piles based on documented field tests by Petek et al. (2016), where $P_\Delta = 5\%D$ is the pile's load capacity corresponding to a settlement equal to 5% of its diameter.

develop $u_e = 0$ during shaking. Among many methods (e.g., Youd et al. 2001; Idriss and Boulanger 2008; Robertson 2015; Cetin et al. 2018), the empirical procedure by Idriss and Boulanger (2008) is widely used for performing a liquefaction hazard analysis for a design earthquake loading, typically quantified via an expected magnitude (M_w) and peak ground acceleration (PGA). These are used to estimate the imposed demand in terms of cyclic stress ratio (CSR) in the various soil layers. The available strength of soil is quantified via liquefaction-triggering correlations that correlate the soil's penetration resistance (either with a standard penetration test N_{160cs} or cone penetration test q_{c1Ncs} values) to a cyclic resistance ratio (CRR). The factor of safety against liquefaction [$FS_{\text{liq}} = (CRR/CSR)$] is computed to categorize the layers as "liquefied" (with $FS_{\text{liq}} \le 1$) and "non-liquefied" (with $FS_{\text{liq}} > 1$). Fig. 4(a) shows FS_{liq} and the interpreted soil layers as liquefied and non-liquefied layers. It should be noted that the identification of layers, whether liquefied or non-liquefied, is always in reference to the design earthquake loading. A layer initially identified as non-liquefied for a given shaking event can still get liquefied under a stronger shaking event. The FS_{liq} computed was used in Step (c) to estimate the peak excess pore pressures (u_e^{pk}) and Step (d) to estimate soil settlement from reconsolidation.

Evaluation of Surface Manifestation Potential

During shaking, liquefaction can result in manifestation in the form of the ejecta of liquefied material reaching the ground surface (Hutabarat and Bray 2021). Ejecta can travel through the interface of the pile (e.g., interface gaps developed from shaking [Fig. 1(c)]) and decrease the pile's shaft resistance. Caltrans' (2020) design procedures use Ishihara's (1985) chart to assess the potential for surface manifestation as a function of the depth and thickness of the liquefied layer and assume zero shaft resistance in all layers affected by the surface manifestation to determine the pile capacity under seismic loading. However, the Caltrans (2020) procedure assumes 100% shaft capacity during reconsolidation, even for layers affected by surface manifestation. Fig. 4(c) illustrates the manifestation-affected layers. The new design procedure also conservatively assumed the extremes of zero shaft capacity in the manifestation-affected layers during shaking but assumes a time-varying shaft capacity as a function of r_u and t_{ult}^o [see Eq. (1)] during reconsolidation (i.e., for liquefaction-induced downdrag).

Peak Excess Pore Pressure Estimation

Significant excess pore pressures (u_e) can generate quickly in liquefiable layers during earthquake loading. While it is expected to develop smaller u_e in the non-liquefied layers, it could increase due to the migration of pore pressure from the adjacent liquefied layers. Estimating the peak excess pore pressures (u_e^{pk}) from earthquake loading, considering redistribution is thus essential for evaluating the minimum shaft and tip capacity following a shaking event. Fig. 4(c) illustrates u_e^{pk} in the soil layers. Sinha et al. (2023) developed an approximate procedure to estimate peak excess pore pressures in liquefied (u_{e-Lu}^{pk}) and non-liquefied (u_{e-NLu}^{pk}) layers considering redistribution. The subscript "Lu" and "NLu" refers to a liquefied layer ("L") and non-liquefied ("NL") under a given undrained loading ("u") condition, such as during an earthquake shaking. The procedure first estimated the earthquake-induced excess pore pressure (u_e^u) (with a superscript "u" referring to undrained loading condition) considering no pore pressure redistribution between the adjacent layers [refer to Eq. (3)]. The estimated u_e^u was then used for computing u_e^{pk} [refer to Eq. (4)] considering redistribution effects from the adjacent layers by accounting for their relative thickness, compressibility, depth, and effective stress.

The earthquake-induced excess pore pressures in the liquefied (u_{e-Lu}^u) and non-liquefied (u_{e-NLu}^u) layers were calculated using FS_{liq} computed in Step (a) as

$$u_{e-Lu}^u (or\ u_{e-NLu}^u) = \sigma'_{vo} \begin{cases} \frac{2.0}{\pi} \arcsin\left(FS_{\text{liq}}^{-\frac{1}{2b\beta}}\right), & FS_{\text{liq}} > 1 \\ 1.0, & FS_{\text{liq}} \le 1 \end{cases} \quad (3)$$

where σ'_{vo} = initial mean effective stress; and b and β = parameters in terms of q_{c1Ncs} and N_{160cs} defined by Mele et al. (2021).

Eq. (4) summarizes the functional form for estimating u_e^{pk} in the liquefied and non-liquefied layers. Sinha et al. (2023) describes all the equations behind these functional forms. The peak excess pore pressure in the liquefied layer (u_{e-Lu}^{pk}) was taken equal to its mean effective stress (σ'_{vo-Lu}). The peak excess pore pressure in the non-liquefied layer (u_{e-NLu}^{pk}) depends upon the layer's initial mean effective stress (σ'_{vo-NLu}) and earthquake-induced excess pore pressure (u_{e-NLu}^u), the relative compressibility ratio [$\overline{m_v} = (m_{v-Lu}/m_{v-NLu})$] and layer thickness ratio [$\bar{H} = (H_{NLu}/H_{Lu})$] with the adjacent liquefied layer and the depth (Z) to the top of the non-liquefied layer [$\bar{Z} = (Z/H_{Lu})$]

$$\begin{aligned} u_{e-Lu}^{pk} &= \sigma'_{vo-Lu} \\ u_{e-NLu}^{pk} &= f(\sigma'_{vo-NLu}, \sigma'_{vo-Lu}, \bar{H}, \overline{m_v}, \bar{Z}, u_{e-NLu}^u) \end{aligned} \quad (4)$$

In Eq. (4), the compressibility (m_v) of the soil layer is computed using relations provided by Seed et al. (1976) and Janbu (1985) as per the procedure described in Sinha et al. (2023) (Fig. 6). The Seed et al. (1976) relation is used to compute the relative compressibility (m_v/m_{vo}) of the soil layers in liquefiable soils depending on the relative density (D_R) and the earthquake-induced excess pore pressure ratio ($r_u^u = u_e^u/\sigma'_{vo}$) as follows:

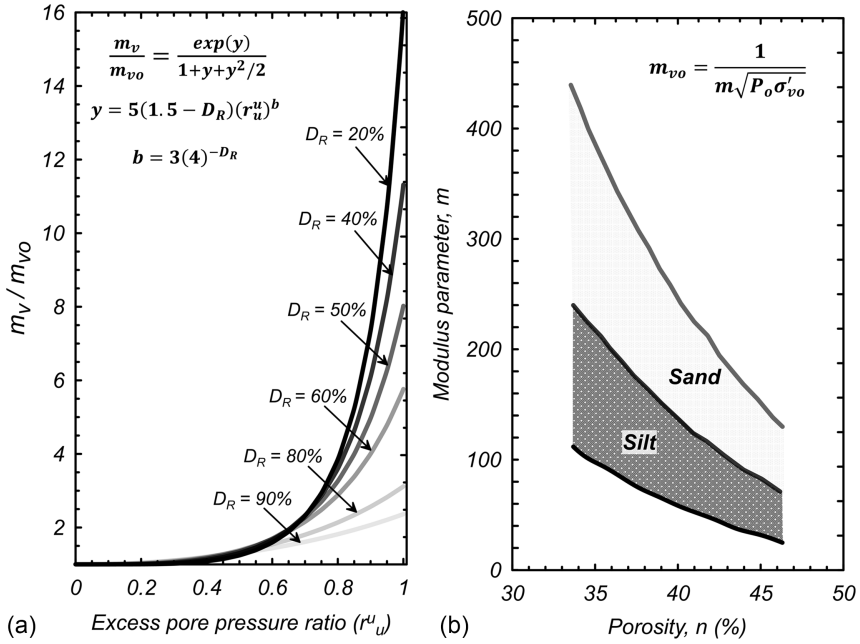

Fig. 6. Estimation of compressibility (m_v) of liquefiable soils using (a) the compressibility ratio (m_v/m_{vo}) relation as a function of earthquake-induced excess pore pressure ratio (r_u^u) from Seed et al. (1976); and (b) compressibility (m_{vo}) of normally consolidated sand and silts at mean effective stress (σ'_{vo}) with ($r_u^u = 0$) from Janbu (1985).

$$\frac{m_v}{m_{vo}} = \frac{\exp(y)}{1 + y + y^2/2}$$
$$y = 5(1.5 - D_R)(r_u^u)^b$$
$$b = 3(4)^{-D_R} \tag{5}$$

where m_{vo} = compressibility at zero excess pore pressure ratio $r_u^u = 0$. The compressibility (m_{vo}) of the normally consolidated sand at mean effective stress (σ'_{vo}) with $r_u^u = 0$ was estimated using empirical correlations from Janbu (1985) as

$$m_{vo} = \frac{1}{m\sqrt{P_{\text{atm}}\sigma'_{vo}}} \tag{6}$$

where m = modulus parameter depending on the porosity (n) of the sand layer (determined from Fig. 6); and P_{atm} = atmospheric pressure, 101.3 kPa. The complete procedure for estimating u_e^{pk} in layered soil deposits are described in detail in Sinha et al. (2023) and Sinha (2022).

Reconsolidation Settlement Estimations

The proposed procedure requires determining the settlement distribution due to post-liquefaction reconsolidation. Several empirical methods, such as Tokimatsu and Seed (1984), Shamoto et al. (1998), Wu (2002), and Idriss and Boulanger (2008), have been developed for estimating reconsolidation settlement; however, their accuracy varies between 25% and 50% (Tokimatsu and Seed 1984). Darby (2018) conducted several centrifuge tests on loose and dense sand under multiple earthquake shakings and found that the estimated reconsolidation settlement using the empirical procedures overestimated the observed measurements. An overestimated reconsolidation settlement would be conservative for pile design. Further research could lead to improved estimates of reconsolidation settlements. Among all available methods, the empirical method from Idriss and Boulanger (2008) was selected to be consistent with the liquefaction hazard analysis. In the section "Comparison of Estimated Pile Settlement and Drag Load With Centrifuge Test" of the present paper, a study is performed to evaluate the effect of reconsolidation settlement on drag load and the associated downdrag settlement in a pile. Fig. 4 illustrates the estimated reconsolidation soil settlement profile corresponding to the liquefaction hazard analysis of Fig. 4(a).

Pile Settlement Estimation

The pile settlement during seismic loading (Stage 2) and due to liquefaction-induced downdrag (Stage 3) was estimated by performing a TzQzLiq analysis [Fig. 4(e)]. The analysis was performed in three stages. Stage 1 models the initial condition with zero excess pore pressures (i.e., $u_e = 0$). Stage 2 models the earthquake shaking period, where u_e is increased linearly from 0 to u_e^{pk} (evaluated in Step c) followed by the application of seismic loads. Stage 3 models the reconsolidation period, where u_e is decreased linearly from u_e^{pk} to 0. Consequently, with the linear decrease of u_e, the reconsolidation soil settlement is increased linearly (see Fig. 3). The pile's shaft capacity and tip capacity were modeled as a function of the excess pore pressure ratio (r_u) as shown in Eq. (1). The effect of surface manifestation on the pile's shaft resistance was modeled by considering the manifestation-affected layers as liquefiable layers, which liquefy during shaking (i.e., $r_u = 1.0$), resulting in zero shaft capacity and reconsolidate post shaking resulting in shaft capacity equal to $(1 - r_u)$ times the ultimate shaft capacity [see Eq. (1)]. The TzQzLiq analysis provides pile settlement and drag load results, which are ultimately used to obtain design curves for the piles [see Fig. 4(f) and Step (f)]. Input parameters for the TzQzLiq numerical model include the pile cross section and material properties, pile head loads (Q_f), profiles of effective stress and soil settlement, and the TzLiq and QzLiq material properties. Cross section and material properties were obtained from the dimension of the pile and the material selected for the design. The load Q_f is the design load applied to the pile's

head during the seismic loading and liquefaction-induced downdrag (see section "Displacement-Based Design Method"). Profiles of effective stress and soil settlement were obtained from Steps (c) and (d), respectively. The TzLiq and QzLiq properties were estimated and calibrated against the pile load test (see section "TzQzLiq Material Properties").

Pile Design Curves

The design curve of the pile comprises the pile settlement (i.e., the head settlement) and drag load for different lengths of the pile [Fig. 4(f)]. Multiple TzQzLiq analyses for different lengths of the piles are performed to obtain the design curves. Fig. 4(f) shows the settlement of the pile at the end of seismic loading as % of its diameter (Stage 2) and the end of liquefaction-induced downdrag (Stage 3), as well as the drag load developed on the pile (at the end of Stage 3) for varying pile lengths (y-axis). Under the same loading conditions, the pile settlement decreases as the pile length increases. On the other hand, the drag load increases and reaches a saturation equal to the shaft resistance above the deepest reconsolidated layer.

The design length of the pile is selected from the design curve based on a serviceability criterion on pile settlement. Typically, the allowable settlement is based on the level of movement that the structure can tolerate. Structures such as long-span bridges may accommodate significant pile settlement without risk of collapse (Law and Wilson 2017). For large diameter piles such as CIDH piles, the serviceability criterion on pile settlement for extreme events generally may be in the range of 5%–10% of the pile's diameter. For some structures, the settlement of the pile relative to the ground could serve as the serviceability criterion. For example, the post-earthquake functionality of the superstructure may be better if the pile settlement is closer to the free-field soil settlement (Sinha et al. 2022b). Fig. 4(f) illustrates the selection of pile design length for an assumed serviceability criterion. With the selected design length of the pile, the design drag load (Q_{drag}) was then estimated. The maximum load acting on the pile $Q_{np} = Q_{dead} + Q_{drag}$ [see Fig. 1(f)] was then checked against the pile's structural strength. If the maximum load exceeds the structural strength of the pile, then the cross section of the pile or its material strength properties are revised, and an associated new design curve is evaluated.

Comparison of Proposed Design Procedure with Centrifuge Tests

The proposed design procedure was applied on piles used in centrifuge model tests SKS02 (Sinha et al. 2021a) and SKS03 (Sinha et al. 2021b) for selected shaking events EQM_3 and EQM_4, respectively. The following subsections briefly describe the centrifuge model tests and the analysis using the proposed design procedure and compare the estimated drag load and pile settlement with centrifuge data.

Description of Centrifuge Model Tests

The tests were performed on the 9-m-radius centrifuge at the Center for Geotechnical Modeling (CGM) at the University of California Davis at a centrifugal acceleration of 40 g. The units reported for the centrifuge test are in the prototype scale following centrifuge scaling laws by Garnier et al. (2007). The centrifuge models consisted of 21 m of the soil profile with an undrained boundary condition underneath due to the impermeable base of the model container. The relative position of the soil layers with their thicknesses for the centrifuge model tests SKS02 and SKS03 are shown in Fig. 7. Table 1 summarizes the soil layer properties for the two centrifuge tests. The soil profile of the centrifuge model test SKS02 consisted of a 9-m-thick liquefiable loose sand layer with relative density ($D_R \approx 43\%$) and porosity ($n \approx 0.41$) sandwiched between

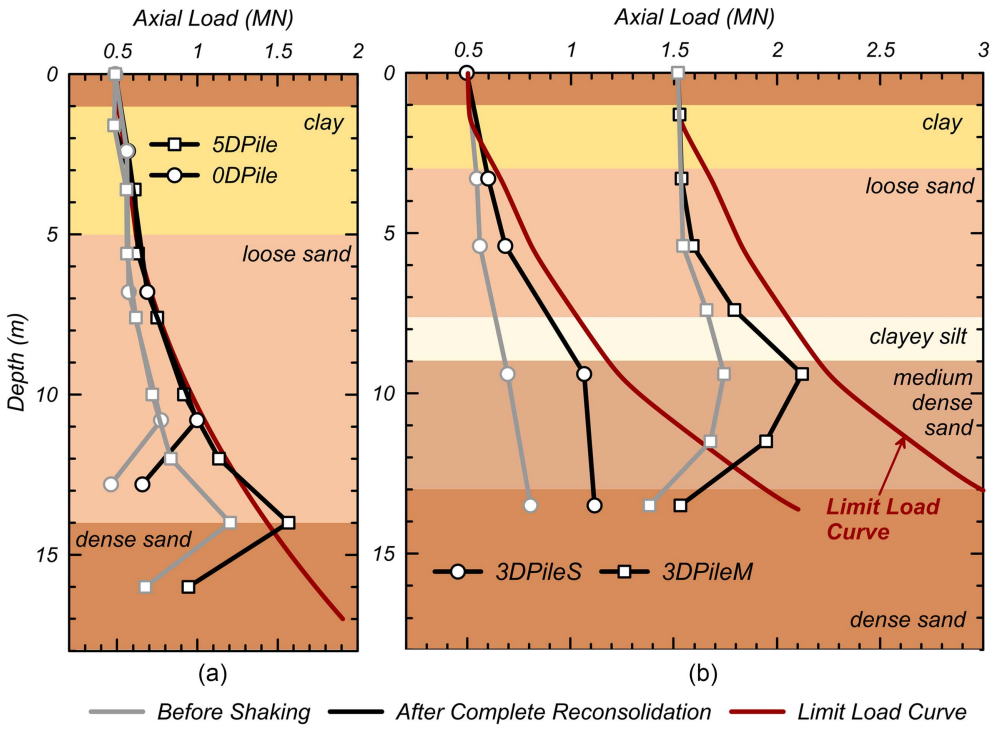

Fig. 7. Axial load distribution in piles before and after shaking, and their corresponding limit load curve for shaking events: (a) EQM_3 (in centrifuge model test SKS02); and (b) EQM_4 (in centrifuge model test SKS03).

Table 1. Soil layer properties in the two centrifuge model tests

Centrifuge model	Layer	Relative density, D_R[a] (%)	Thickness (m)	Saturated density (kg/m^3)	Shear wave velocity, V_S[b] (m/s)	Permeability, k[c] (cm/s)
SKS02	Monterey sand	95	1	2,054	55	0.04
	Clay	—	2	1,700	75	0.000312
	Loose sand	43	4.7	1,971	160	0.026
	Dense sand	85	1.3	2,000	242	0.026
SKS03	Monterey sand	95	1	2,054	55	0.04
	Clay	—	2	1,700	75	0.000312
	Loose sand	40	4.7	1,971	141	0.026
	Clayey silt	—	1.3	2,000	110	0.00036
	Medium-dense sand	60	4	1,019	195	0.022
	Dense sand	86	8	2,051	250	0.022

[a]Measured during model construction.
[b]Estimated from the empirical correlations of Baldi et al. (1989), Hegazy and Mayne (1995), Clariá and Rinaldi (2007), and Mayne and Rix (1995).
[c]Scaled to prototype scale.

a 4-m-thick layer of low permeable over-consolidated clay layer (with an undrained shear strength $s_u \approx 20$ kPa) on top and dense sand ($D_R \approx 85\%$) layer below. The soil profile of the centrifuge model test SKS03 consisted of 1 m of Monterey Sand, 2 m of clay crust ($s_u \approx 28$–35 kPa), 4.7 m of a loose liquefiable sand layer ($D_R \approx 40\%$, $n \approx 0.41$), 1.3 m of a clayey silt layer (20% clay and 80% silt), 4 m of a medium-dense sand layer ($D_R \approx 60\%$, $n \approx 0.39$), and a dense sand layer ($D_R \approx 86\%$, $n \approx 0.36$). The effective unit weight (γ') of the sand layer was about 10 ± 0.1 kN/m^3.

The models consisted of identical pipe piles of aluminum with an outer diameter (D) of 635 mm and a thickness of 35 mm. The centrifuge model test SKS02 consisted of two piles: 0DPile and 5DPile, both with a dead load of $Q_{\text{dead}} = 500$ kN, resulting in a static factor of safety of 5.4 and 12.4, respectively. The centrifuge model test SKS03 consisted of three piles: 3DPileS, 3DPileM, and 3DPileL with a dead load of $Q_{\text{dead}} = 500$ kN, 1,500 kN, and 2,400 kN with a static factor of safety of 8, 2.6, and 1.6, respectively. The 0D, 3D, and 5D naming annotations indicate the embedment depth of the pile's tip, i.e., the 0DPile had its tip placed at the bottom of the loose sand layer. The annotations S, M, and L in 3DPiles correspond to the small, medium, and large dead loads applied to the piles.

The models were shaken with multiple scaled Santa Cruz earthquake motions of $M_w = 6.9$ from the Loma Prieta 1989 earthquake. Shaking event EQM_3 was the third shaking event in sequence applied to the centrifuge model SKS02 with a peak base acceleration (PBA) of 0.24 g. Shaking event EQM_4 was the fourth shaking event in sequence applied to the centrifuge model SKS03. It was a long duration modified Santa Cruz motion (Malvick et al. 2002) consisting of one large pulse followed by five small pulses, scaled to produce a PBA of 0.45 g.

The models were instrumented with accelerometers, strain gauges on piles, pore pressure transducers, and settlement sensors to monitor accelerations on piles, the generation of excess pore pressures, and soil and pile settlement. The normalized overburden corrected cone tip resistance ($q_{c1Ncs} = C_N q_c / P_a$), peak excess pore pressure (u_e^{pk}), and soil settlement profile measured during the shaking events EQM_3 and EQM_4 are shown later in Figs. 8(a, c, and d) and 9(a, c, and d), respectively. The q_{c1Ncs} profile was interpreted from the cone penetration test (CPT) conducted in the centrifuge (Sinha et al. 2021a, b). Thin layer effects were accounted for by ignoring q_c close to the transition near the top and bottom of each layer (Khosravi et al. 2022). While the sand layers were placed uniformly during construction, following the empirical procedure of overburden correction (C_N) by Idriss and Boulanger (2008) resulted in computed q_{c1ncs} slightly varying with depth, suggesting either an increase in D_R (about 10%) with depth and/or a discrepancy between C_n applicable to our mini-cone tests in the centrifuge and field-scale cone tests in calibration chambers upon which the empirical procedures are based. The CPTs in the centrifuge are a good indicator of changes in soil densities (Bolton et al. 1999; Darby et al. 2019; Kutter et al. 2020); however, their interpretation using C_N factor is not unique but depends on the soil density, sand properties, and cone to particle diameter ratio (Boulanger 2003). Profiles of u_e^{pk} are the peak excess pore pressure profile recorded during the shaking event [Figs. 8(c) and 9(c)]. The soil settlement profile [Figs. 8(d) and 9(d)] was estimated from the inverse analysis of measured u_e in the centrifuge test (Sinha et al. 2022b). The initial (i.e., before shaking) and final (i.e., at the end of reconsolidation) axial load distributions of the piles are shown in Fig. 7. The figure shows that the piles had an initial drag load developed from the prior shaking events. After complete reconsolidation, the drag load on the piles and the axial load at all depths increased. During shaking, the piles: two 3DPiles (3DPileS and 3DPileM), the 0DPile, and the 5DPile experienced a vertical acceleration of 0.1 g, 0.25 g, and 0.03 g, respectively. The limit load curve for the piles, defined as axial load distribution for maximum drag load developed on the pile, is shown in Fig. 7 (Sinha et al. 2022b). The limit load curve is obtained from the summation of the pile head load and the cumulative integration of the pile's interface shear strength with depth, assuming the pile mobilizes negative skin friction equal to its interface shear strength. The measured settlement of the piles during shaking and due to liquefaction-induced downdrag are listed in Table 2.

Analysis Using Proposed Design Procedure

The simplified liquefaction-triggering procedures of Idriss and Boulanger (2008) and others typically use the input as the maximum ground surface acceleration (PGA) that would have occurred if the site did not liquefy (Allmond 2012; Olson et al. 2020). Since the ground surface acceleration measured in the centrifuge tests was affected by the liquefaction, the use of the measured motion is not, in general, the appropriate input for the liquefaction evaluation in the experiment. Instead, a one-dimensional equivalent linear analysis (EQL) with no pore pressure generation was performed in DEEPSOIL (Hashash et al. 2020) to estimate PGA that could be used with the liquefaction-triggering procedure. The soil layer properties used in the analysis are summarized in Table 1.

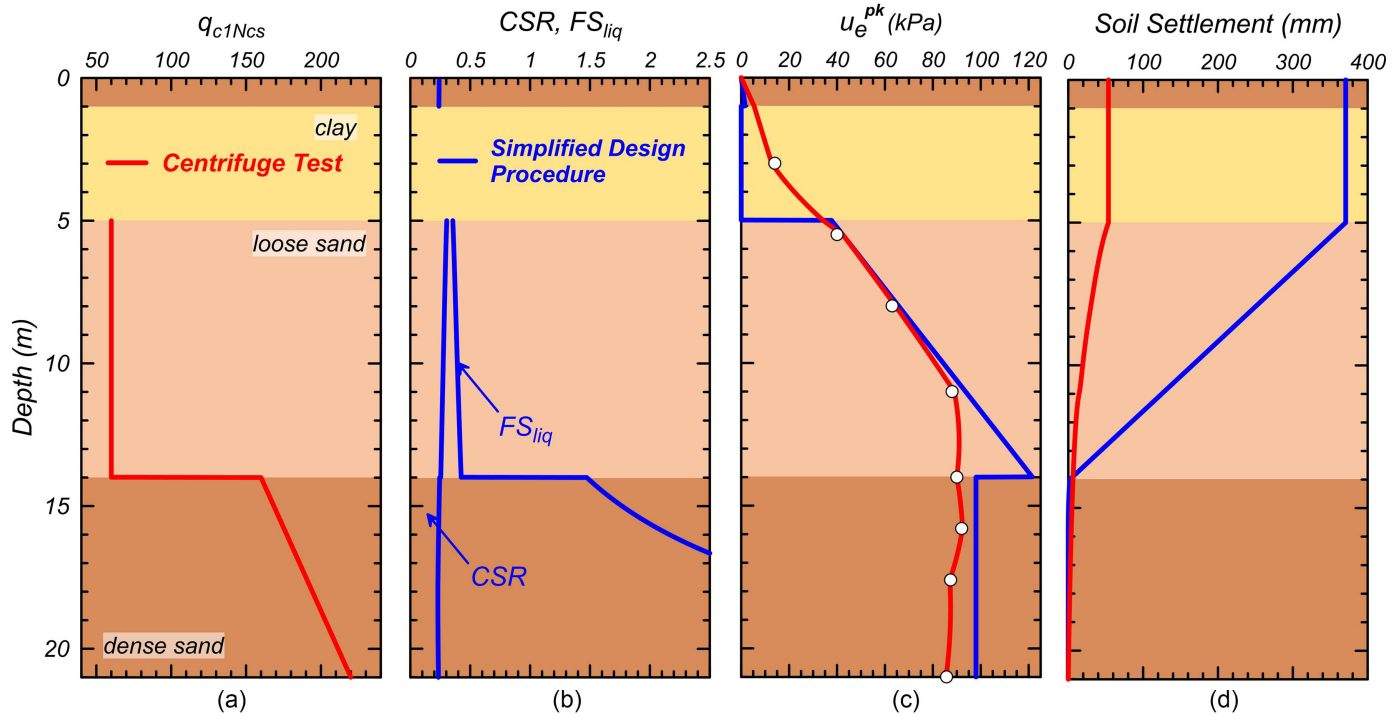

Fig. 8. Results from the proposed design procedure for shaking event EQM_3 in centrifuge model test SKS02 with (a) normalized overburden corrected cone tip resistance (q_{c1Ncs}); and (b) cyclic stress ratio (CSR) resulting in a factor of safety against liquefaction (FS_{liq}). Comparison of (c) estimated peak excess pore pressures profile against measurements from pore pressure transducers; and (d) estimated soil settlement profile against soil settlement profile obtained from the inverse analysis of measured excess pore pressures. (Data from Sinha et al. 2022c.)

Empirical correlations using cone tip resistance (Hegazy and Mayne 1995; Clariá and Rinaldi 2007; Mayne and Rix 1995; Baldi et al. 1989) were used to estimate the shear wave velocity (V_S) of the soil layers (see Table 1). The soil models used were the shear modulus and damping curves obtained from Seed and Idriss (1970) (for the sand layers) and Vucetic and Dobry (1991) (for clay and clayey silt layers). The PGA obtained from the analysis for the two shaking events, EQM_3 and EQM_4, was 0.23 g and 0.16 g, respectively.

The cyclic stress ratio (CSR), the factor of safety against liquefaction (FS_{liq}), peak excess pore pressure (u_e^{pk}), and soil settlement profiles obtained for the shaking events EQM_3 and EQM_4 following the proposed design procedure are shown in Figs. 8 and 9, respectively. The figures also compare the estimated u_e^{pk} with the measurements from pore pressure transducers; and the reconsolidated soil settlement profile with the settlement profile obtained from the inverse analysis of measured excess pore pressures. The subsections below briefly describe the soil liquefaction hazard analysis, estimated peak excess pore pressure, and soil settlement profile for the two shaking events and their comparison with the centrifuge test, while a separate subsection describes the TzQzLiq analysis of piles using the estimated u_e^{pk} and soil settlement profiles.

Soil Liquefaction Hazard Analysis

A liquefaction hazard analysis of centrifuge model tests SKS02 and SKS03 for shaking events EQM_3 and EQM_4 was performed using the CPT-based (q_{c1Ncs}) liquefaction-triggering correlation procedures from Idriss and Boulanger (2008). For EQM_3 in SKS02, the liquefaction-triggering correlation procedure estimated liquefaction ($FS_{liq} \leq 1$) in the loose sand layer between 5–14 m (Fig. 8). For EQM_4 in SKS03, liquefaction was estimated in the loose sand layer and the upper 1.6 m of the thick medium-dense sand layer (Fig. 9). The non-liquefied layers ($FS_{liq} > 1$) consisted of the dense sand layer below 14 m in SKS02 and the medium-dense and dense sand below 10.7 m in SKS03. Empirical curves from Ishihara (1985) predicted no surface manifestation. The predictions were consistent with the results from the centrifuge tests.

The peak excess pore pressure u_e^{pk} in the non-liquefied layers was estimated considering the redistribution effects. The peak excess pore pressures in the soil layers estimated for the selected shaking events EQM_3 and EQM_4 are shown in Figs. 8(c) and 9(c), respectively. For EQM_3 in SKS02, the u_e^{pk} in the non-liquefied layer was estimated for a compressibility ratio of ($\overline{m_v} = 20$), the thickness ratio of ($\bar{H} = 0.78$), depth to the top of the non-liquefied layer ($Z = 14$ m), and the average earthquake-induced excess pore pressure ratio in the non-liquefied layer ($r^u_{u-NLu} = 0.096$). For EQM_4 in SKS03, the parameters included $\overline{m_v} = 12$, $\bar{H} = 5.6$, $Z = 10.8$ m, and $r^u_{u-NLu} = 0.24$. The peak excess pore pressures estimated in the non-liquefied layers were $u^{pk}_{e-NLu} = 98$ kPa and $u^{pk}_{e-NLu} = 74$ kPa in SKS02 and SKS03, respectively [Figs. 8(c) and 9(c)]. The estimated u_e^{pk} in the non-liquefied layers match pretty well with the pore pressure transducer measurements.

Soil Settlement from Reconsolidation

The estimated soil settlement profile using the empirical procedures from Idriss and Boulanger (2008) for EQM_3 and EQM_4 are shown in Figs. 8(d) and 9(d), respectively. The figures also include the soil settlement profile obtained by performing an inverse analysis of measured excess pore pressures and validated against surface settlement measurements (Sinha et al. 2022c). From the figures, it can be seen that the empirical procedures predicted significantly higher (>400%) magnitudes of soil settlement (in the loose and medium-dense sand layers) compared to the estimated settlement from the inverse analysis. At the same time, the estimated soil settlement underpredicted settlements in the dense sand layers.

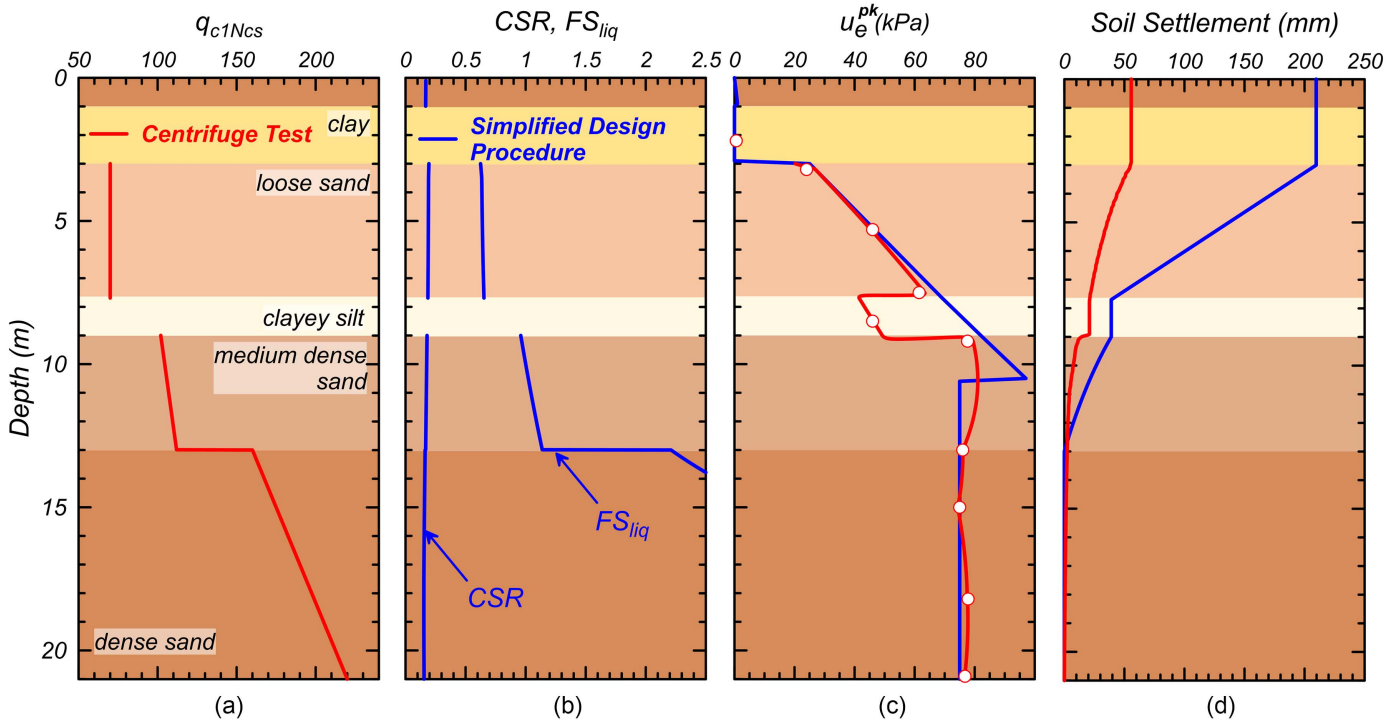

Fig. 9. Results from the proposed design procedure for shaking event EQM_4 in centrifuge model test SKS03 with (a) normalized overburden corrected cone tip resistance (q_{c1Ncs}); and (b) cyclic stress ratio (CSR) resulting in a factor of safety against liquefaction (FS_{liq}). Comparison of (c) estimated peak excess pore pressures profile against measurements from pore pressure transducers; and (d) estimated soil settlement profile against soil settlement profile obtained from the inverse analysis of measured excess pore pressures. (Data from Sinha et al. 2022c.)

For both shaking events [Figs. 8(d) and 9(d)], the soil settlement profile from the inverse analysis showed some small settlements in dense layers. The estimated soil settlement from the inverse analysis (Sinha et al. 2022c) at the tip of 0DPile, 5DPile, and 3DPiles was about 6, 3, and 1.5 mm, respectively. In contrast, Idriss and Boulanger's (2008) empirical procedure estimated no settlement in the dense sand layer. Soil settlements in the dense sand layers and near the pile's tip can significantly affect the settlement of the pile and the development of drag loads. Sinha et al. (2019) studied the effect of reconsolidation strains near the pile's tip and found that it results in more drag loads and pile settlement. TzQzLiq analyses were performed for the two soil settlement profiles to investigate the effect of reconsolidation strains in the dense sand on pile settlement and drag load and are described in what follows.

TzQzLiq Analysis of Piles

A TzQzLiq analysis of the piles was performed in OpenSees (McKenna et al. 2010) with a mesh discretization of 0.1 m. The latest version of OpenSees (available from the GitHub repository at https://github.com/OpenSees/OpenSees) with the QzLiq material model implemented was used to perform the analysis. The properties of the TzLiq and QzLiq materials used in the analysis are summarized in Table 2 of Sinha et al. (2022c). The material properties were calibrated against limit load curves and pile load test results obtained from the centrifuge tests (Sinha et al. 2022c). Load transfer backbone curves from Reese and O'Neil (1987) and Mosher (1984) were used to model the TzLiq material behavior in sand and clay layers, respectively. The QzLiq load transfer behavior was modeled with backbone curves from Vijivergiya (1977). The ultimate capacity of TzLiq at different depths along the length of the pile was obtained from the limit load curves shown in Fig. 7. The stiffness parameter (z_{50}) of TzLiq was taken as 0.3% of the pile's diameter in the clay, silt, loose sand, and medium-dense sand layers and 0.15% of the pile's diameter in the dense sand layer. The QzLiq material parameters [capacity ($q^o_{t,\mathrm{ult}}$) and stiffness (z_{50})] were calibrated against pile load test results. The constant α_t was taken as 0.55, calculated using Eq. (1) with an effective friction angle of $\phi' = 30°$. The piles' seismic loads were calculated from the maximum vertical acceleration experienced during shaking and were 125, 15, 50, and 150 kN for the 0DPile, 5DPile, 3DPileS, and 3DPileM, respectively.

While many empirical methods exist for estimating soil settlement profiles, they may not predict soil settlements accurately at all depths. Since the downdrag phenomenon depends upon the reconsolidated soil profile, it is essential to study the effect of two critical parameters: (1) the magnitude of overall soil settlement; and (2) the soil settlement at the pile's tip on the development of drag load and downdrag settlement. A sensitivity study on the magnitude of reconsolidation soil settlement on drag load and pile settlement was performed by analyzing multiple soil settlement profiles scaled to produce surface settlements in the range of 10–400 mm. Additionally, two types of TzQzLiq analyses (denoted henceforth as I and II) were performed to study the effect of reconsolidation strains in the dense sand layer and near the pile's tip. TzQzLiq I used the soil settlement profile estimated from the inverse analysis of measured excess pore pressures described in Sinha et al. (2022c). TzQzLiq II used the soil settlement profile estimated by Idriss and Boulanger (2008) scaled to produce surface settlement equal to the measurement in the centrifuge test. Finally, a TzQzLiq analysis using the proposed design procedure (i.e., TzQzLiq II with an unscaled soil settlement profile) named "Proposed Design Procedure" was performed, and the results were compared with the centrifuge test. All other components of the three analyses were identical.

Table 2. Comparison of pile settlement and drag load results obtained from the TzQzLiq analyses of 0DPile, 5DPile, and the 3DPiles (3DPileS, 3DPileM, and 3DPileL) for shaking event EQM_3 in centrifuge model test SKS02 and shaking event EQM_4 in centrifuge model test SKS03 respectively, against the measurements from each centrifuge test

Pile	Methods	Soil settlement		Pile settlement (%D)		Drag load (kN)
		Surface (mm)	At the tip (%D)	Seismic	Downdrag	
0DPile	Centrifuge test	54	1.0	1.7	1.4	498
	TzQzLiq I[a]	54	1.0	Pile plunged into the soil due to loss of tip resistance ($r_u \approx 1.0$ near the tip)		
	TzQzLiq I[b]	54	0			
	Proposed design procedure[c]	370	0			
5DPile	Centrifuge test	54	0.4	0.0	0.8	1,068
	TzQzLiq I[a]	54	0.4	0.0	0.8	527
	TzQzLiq I[b]	54	0.0	0.0	0.3	690
	Proposed design procedure[c]	370	0.0	0.0	0.6	1,024
3DPileS	Centrifuge test	56	0.2	0.3	0.6	600
	TzQzLiq I[a]	56	0.2	0.1	0.8	641
	TzQzLiq I[b]	56	0.0	0.1	0.5	597
	Proposed design procedure[c]	212	0.0	0.1	1.4	1,127
3DPileM	Centrifuge test	56	0.2	4.4	0.9	620
	TzQzLiq I[a]	56	0.2	3.5	0.9	672
	TzQzLiq I[b]	56	0.0	3.5	0.7	674
	Proposed design procedure[c]	212	0.0	3.5	1.7	1,021
3DPileL	Centrifuge test	56	0.2	31.5	1.1	—
	TzQzLiq I[a]	56	0.2	21.1	0.9	686
	TzQzLiq I[b]	56	0.0	21.1	0.7	699
	Proposed design procedure[c]	212	0.0	21.1	1.7	1,032

[a]TzQzLiq Analysis with soil settlement profile estimated from the inverse analysis of measured excess pore pressures (Sinha et al. 2022c).
[b]TzQzLiq Analysis with soil settlement profile estimated from Idriss and Boulanger (2008) and scaled to get a surface settlement equal to measured surface settlement in centrifuge test.
[c]TzQzLiq Analysis using Proposed Design Procedure with soil settlement profile estimated from Idriss and Boulanger (2008).

Comparison of Estimated Pile Settlement and Drag Load with Centrifuge Test

The TzQzLiq analysis is shown to produce a reasonable estimate of the seismic settlement of piles. The comparison of the seismic settlement of the piles with measurements from the centrifuge test is shown in Table 2. Since all the different TzQzLiq analyses (TzQzLiq I, TzQzLiq II, and Proposed Design Procedure) had the same excess pore pressure profiles and seismic loads, their results on the seismic settlements were the same. The TzQzLiq analysis predicted the plunging of 0DPile due to the excess pore pressure ratio reaching $ru = 1.0$ around its tip. Contrary to that, the centrifuge test showed no plunging failure and resulted in the seismic settlement of about 1.7% D. The penetration of the 0DPile's tip to the dense sand layer (during shaking) could have provided additional tip resistance leading to a smaller seismic settlement. The estimated seismic settlement for the deeply embedded 5DPile with a small dead load was negligible, similar to centrifuge test recordings. The estimated seismic settlement for all 3DPiles was slightly smaller than the measured settlements. The predicted seismic settlement in the 3DPileS, 3DPileM, and 3DPileL were about 0.1% D, 3.5% D, and 21.1% D compared to the measured settlement of 0.3% D, 4.4% D, and 31.5% D, respectively. The difference in the result could be due to the multiple cycles of seismic load occurring on the piles, compared to the single cycle of seismic load applied in the TzQzLiq analysis. A separate analysis showed that ten cycles of seismic load on 3DPileM could predict seismic settlements equal to the settlements observed in the centrifuge test. Like the centrifuge test, TzQzLiq analysis showed a substantial settlement of 3DPileL (>20% D), indicating the plunging of the pile into the soil. The difference in the seismic settlement prediction for 3DPileL is due to the inability of the TzQzLiq analysis to model pile settlement during plunging.

The estimated downdrag settlement in the piles from the TzQzLiq analyses matched reasonably well with the centrifuge tests. The downdrag settlement for the different magnitudes of soil settlement profile is shown in Fig. 10. The TzQzLiq analyses showed an increase in downdrag settlement with the magnitude of soil settlement and settlement in the dense sand layers. For example, for 3DPileS, downdrag settlement increased from 0% to about 1.5% of the pile diameter when the soil settlement increased from 10 to 370 mm. Overall for all the piles (5DPile and 3DPiles), the resulting downdrag settlement was small and was within 2% of the pile's diameter. Results on downdrag settlement from the three TzQzLiq analyses and their comparison with the centrifuge test are summarized in Table 2. Results show that for the same magnitude of soil settlement, the downdrag settlement is higher if there are soil settlements near the pile tip (Sinha et al. 2019). TzQzLiq I (which had soil settlement at the pile's tip) consistently showed higher downdrag settlement than TzQLiq II (which had no soil settlement at the pile's tip). The downdrag settlement of TzQzLiq I with the soil settlement profile estimated from the inverse analysis matched quite well with the centrifuge test results. The downdrag settlement results from TzQzLiq analysis following the proposed design procedure were found to be conservative due to the large magnitude of soil settlement predicted from the empirical procedure.

The drag load on piles also increased with soil settlement, but it approached saturation at large magnitudes of settlements (see Fig. 10). For example, for 5DPile, the drag load increased from 100 to 1,000 kN as the soil settlement increased from 10 to

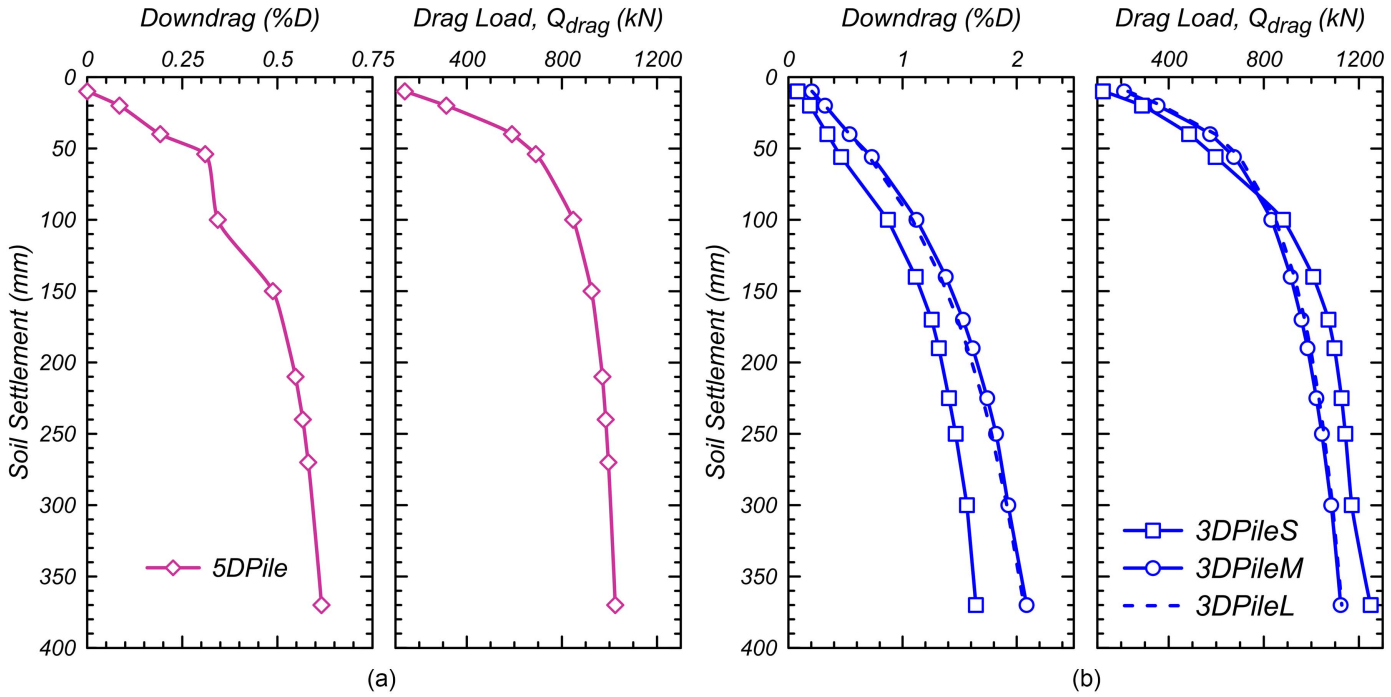

Fig. 10. Results from the proposed design procedure on downdrag settlement and drag load with the magnitude of soil settlement for (a) 5DPile for shaking event EQM3 of the centrifuge model test SKS02; and (b) 3DPileS, 3DPileM, and 3DPileL for shaking event EQM4 of the centrifuge model test SKS03.

370 mm. Among the 3DPiles, the drag load was higher for lightly loaded piles (3DPileS) than heavily loaded piles (3DPileM and 3DPileL). The comparison of drag loads in Table 2 for the three different TzQzLiq analyses showed larger drag loads for a larger magnitude of soil settlement. The TzQzLiq analysis following the proposed design procedure gave conservative estimates of drag load compared to the measured drag loads in centrifuge tests.

Overall, the proposed design procedure analysis of piles used in the centrifuge test provided a reasonable estimate of seismic settlement, downdrag settlement, and drag loads on piles. The majority of the pile settlement was coseismic. Although significant drag loads developed on the piles, the resulting downdrag settlement was small (<2% D). The predictions from TzQzLiq analyses following the proposed design procedure (see Table 2) were conservative compared to the results from the centrifuge test. The conservatism in drag load and downdrag settlement estimates was mainly due to the conservatism in predicting the magnitude of soil settlement from reconsolidation.

Summary and Conclusions

A new displacement-based design procedure using a TzQzLiq analysis was presented for designing axially loaded single piles (with no pile cap effects) for earthquake loading and liquefaction-induced downdrag. Although the proposed procedure is derived from experiments and simulations of single piles, it is likely to be useful for pile groups where spacing is large. The pile cap effects will be minor if the pile cap settlement is less than the ground settlement, as there would likely be a gap under the pile cap. For the case where pile cap settlement is greater than the soil settlement, ignoring pile cap effects would be conservative. The design procedure accounts for the initial drag load (or axial load distribution) on the pile, peak excess pore pressures in the non-liquefied layers following redistribution from the liquefied layers, and the reduction of the shaft and tip capacity from free-field excess pore pressures in the soil around the pile. The design procedure, in total, involves six simplified steps (described in detail in the paper) for obtaining design curves relating to pile settlement and drag loads for varying pile lengths. Finally, using the design curves, a design pile length is selected based on the serviceability criterion of the pile settlement (both absolute and relative to the free-field ground settlement) and its structural strength. The proposed design procedure was applied to analyze piles conducted in centrifuge tests. Results showed that the proposed procedure reasonably predicted the pile's seismic settlement, downdrag settlement, and drag load. Finally, an example problem was presented to demonstrate a step-by-step application of the new design procedure and compare the results with Caltrans' (2020) method (refer to Appendix A). Some of the main conclusions from this paper are as follows:

- Liquefaction-induced downdrag is not the controlling mechanism for pile settlement. While reconsolidation settlement caused large drag loads on piles, the resulting downdrag settlement was small (<2% of pile diameter).
- Most of the pile settlement occurs during shaking. The development of large seismic loads simultaneously with the increased excess pore pressure in the soil, causing the reduction of the pile tip and shaft capacity, is the leading cause of pile settlement in liquefiable soils.
- The pile's tip should be embedded sufficiently from the liquefiable layer to avoid significant loss of tip capacity during shaking. Migration of pore pressure from the liquefied layer can cause increased excess pore pressure in the bearing (non-liquefied) layer, resulting in decreased pile tip capacity and stiffness.

The proposed design procedure captures all the mechanisms during a shaking event and estimates both pile settlement and axial load distribution, resulting in a more informed and safe design. The design pile using the proposed procedure was governed by pile

settlement during seismic shaking as opposed to the drag load using the force-based design procedure by Caltrans (2020) (Appendix A). The proposed design procedure saved pile length (for the considered example design problem) by more than 10% compared to Caltrans' (2020) procedure (Appendix A). Such savings in pile length can significantly reduce the cost of construction projects that involve installing many piles.

Data Availability Statement

Some or all data, models, or code generated or used during the study are available in a repository online under funder data retention policies. The centrifuge test data used in this study are made available through DesignSafe (Sinha et al. 2021a, b).

Acknowledgments

The California Department of Transportation funded this research under Agreement 65A0688. The authors would like to acknowledge the Caltrans engineers (especially Abbas Abghari, Qiang Huang, and Mohammed Islam) involved in this project for their suggestions and assistance. The centrifuge tests were made possible by the Center for Geotechnical Modeling facilities and staff at UC Davis. The centrifuge facility at UC Davis is part of the NSF Natural Hazards Research Infrastructure (NHERI) program under Award CMMI 2037883.

Supplemental Materials

Appendix A, including Tables A1 and A2 and Figs. A1–A3, is available online in the ASCE Library (www.ascelibrary.org).

References

AASHTO. 2011. *AASHTO guide specifications for LRFD seismic bridge design*. AASHTO LRFDSEIS-2. Washington, DC: AASHTO.

AASHTO. 2020. *AASHTO LRFD bridge design specifications*. AASHTO LRFDUS-9. Washington, DC: AASHTO.

Allmond, J. D. 2012. "Shallow rocking foundations in liquefiable and saturated soil conditions." Ph.D. dissertation, Dept. of Civil and Environmental Engineering, Univ. of California, Davis.

Baldi, G., R. Bellotti, V. N. Ghionna, M. Jamiolkowski, and D. C. F. Lo Presti. 1989. "Modulus of sands from CPT's and DMT's." In *Proc., 12th Int. Conf. on Soil Mechanics and Foundation Engineering*, 165–170. Rio de Janeiro, Brazil: International Conference on Soil Mechanics and Foundation Engineering.

Bhattacharya, S., and S. P. G. Madabhushi. 2008. "A critical review of methods for pile design in seismically liquefiable soils." *Bull. Earthquake Eng.* 6 (3): 407–446. https://doi.org/10.1007/s10518-008-9068-3.

Bhattacharya, S., S. P. G. Madabhushi, and M. D. Bolton. 2004. "An alternative mechanism of pile failure in liquefiable deposits during earthquakes." *Géotechnique* 54 (3): 203–213. https://doi.org/10.1680/geot.2004.54.3.203.

Bolton, M. D., M. W. Gui, J. Garnier, J. F. Corte, G. Bagge, J. Laue, and R. Renzi. 1999. "Centrifuge cone penetration tests in sand." *Géotechnique* 49 (4): 543–552. https://doi.org/10.1680/geot.1999.49.4.543.

Boulanger, R. W. 2003. "High overburden stress effects in liquefaction analyses." *J. Geotech. Geoenviron. Eng.* 129 (12): 1071–1082. https://doi.org/10.1061/(ASCE)1090-0241(2003)129:12(1071).

Boulanger, R. W., and S. J. Brandenberg. 2004. "Neutral plane solution for liquefaction-induced downdrag on vertical piles." In *GeoTrans: Geotechnical Engineering for Transportation Projects*, Geotechnical Special Publication 126, edited by M. K. Yegian and E. Kavazanjian, 470–478. Reston, VA: ASCE. https://doi.org/10.1061/40744(154)32.

Boulanger, R. W., C. J. Curras, B. L. Kutter, D. W. Wilson, and A. Abghari. 1999. "Seismic soil-pile-structure interaction experiments and analyses." *J. Geotech. Geoenviron. Eng.* 125 (9): 750–759. https://doi.org/10.1061/(ASCE)1090-0241(1999)125:9(750).

Caltrans. 2020. "Liquefaction-induced downdrag." Accessed February 1, 2020. https://dot.ca.gov/programs/engineering-services/manuals/geotechnical-manual.

Cetin, K. O., R. B. Seed, R. E. Kayen, R. E. S. Moss, H. T. Bilge, M. Ilgac, and K. Chowdhury. 2018. "SPT-based probabilistic and deterministic assessment of seismic soil liquefaction triggering hazard." *Soil Dyn. Earthquake Eng.* 115 (Dec): 698–709. https://doi.org/10.1016/j.soildyn.2018.09.012.

Clariá, J. J., and V. A. Rinaldi. 2007. "Shear wave velocity of a compacted clayey silt." *Geotech. Test. J.* 30 (5): 399–408. https://doi.org/10.1520/GTJ100655.

Darby, K. M. 2018. "The use of centrifuge model studies in the development of CPT-based liquefaction triggering correlations." Ph.D. Dissertation, Dept. of Civil and Environmental Engineering, Univ. of California, Davis.

Darby, K. M., R. W. Boulanger, J. T. DeJong, and J. D. Bronner. 2019. "Progressive changes in liquefaction and cone penetration resistance across multiple shaking events in centrifuge tests." *J. Geotech. Geoenviron. Eng.* 145 (3): 04018112. https://doi.org/10.1061/(ASCE)GT.1943-5606.0001995.

Fellenius, B. H. 1984. "Negative skin friction and settlement of piles." In *Proc., 2nd Int. Seminar, Pile Foundations*, 1–12. Singapore: Nanyang Technological Institute.

Garnier, J., C. Gaudin, S. M. Springman, P. J. Culligan, D. Goodings, D. Konig, B. Kutter, R. Phillips, M. F. Randolph, and L. Thorel. 2007. "Catalogue of scaling laws and similitude questions in geotechnical centrifuge modelling." *Int. J. Phys. Modell. Geotech.* 7 (3): 1–23. https://doi.org/10.1680/ijpmg.2007.070301.

Hashash, Y. M. A., M. I. Musgrove, J. A. Harmon, I. Okan, G. Xing, O. Numanoglu, D. R. Groholski, C. A. Phillips, and D. Park. 2020. *DEEPSOIL 7.0 user manual*. Urbana, IL: Board of Trustees of Univ. of Illinois at Urbana-Champaign.

Hegazy, Y. A., and P. W. Mayne. 1995. "Statistical correlations between Vs and cone penetration data for different soil types." In Vol. 95 of *Proc., of Int. Symp. on Cone Penetration Testing*, 173–178. Linkoping, Sweden: Swedish Geotechnical Society.

Hutabarat, D., and J. D. Bray. 2021. "Effective stress analysis of liquefiable sites to estimate the severity of sediment ejecta." *J. Geotech. Geoenviron. Eng.* 147 (5): 04021024. https://doi.org/10.1061/(ASCE)GT.1943-5606.0002503.

Idriss, I. M., and R. W. Boulanger. 2008. *Soil liquefaction during earthquakes*. Oakland, CA: Earthquake Engineering Research Institute.

Ishihara, K. 1985. "Stability of natural deposits during earthquakes." In *Proc., 11th Int. Conf. on Soil Mechanics and Foundation Engineering*, 321–376. San Francisco: International Conference on Soil Mechanics and Foundation Engineering.

Janbu, N. 1985. "Soil models in offshore engineering." *Géotechnique* 35 (3): 241–281. https://doi.org/10.1680/geot.1985.35.3.241.

Kaynia, A. M. 2022. *Analysis of pile foundations subject to static and dynamic loading*. London: CRC Press. https://doi.org/10.1201/9780429354281.

Kim, H.-J., and J. L. C. Mission. 2011. "Development of negative skin friction on single piles: Uncoupled analysis based on non-linear consolidation theory with finite strain and the load-transfer method." *Can. Geotech. J.* 48 (6): 905–914. https://doi.org/10.1139/t11-004.

Knappett, J. A., and S. P. G. Madabhushi. 2009. "Seismic bearing capacity of piles in liquefiable soils." *Soils Found.* 49 (4): 525–535. https://doi.org/10.3208/sandf.49.525.

Kutter, B. L., M. T. Manzari, and M. Zeghal. 2020. *Model tests and numerical simulations of liquefaction and lateral spreading: LEAP-UCD-2017*. Cham, Switzerland: Springer. https://doi.org/10.1007/978-3-030-22818-7.

Lam, S. Y., C. W. W. Ng, C. F. Leung, and S. H. Chan. 2009. "Centrifuge and numerical modeling of axial load effects on piles in consolidating

ground." *Can. Geotech. J.* 46 (1): 10–24. https://doi.org/10.1139/T08-095.
Law, H., and P. Wilson. 2017. "Displacement based downdrag analysis for pile design." In *Proc., 3rd Int. Conf. on Performance Based Design (PBD-III)*. Vancouver, BC, Canada: International Conference on Soil Mechanics and Foundation Engineering.
Madabhushi, G., J. Knappett, and S. Haigh. 2010. *Design of pile foundations in liquefiable soils*. London: Imperial College Press. https://doi.org/10.1142/p628.
Malvick, E. J., R. Kulasingam, R. W. Boulanger, and B. L. Kutter. 2002. *Effects of void redistribution on liquefaction flow of layered soil—Centrifuge data report for EJM01*. Rep. No. UCD/CGMDR-02/02. Davis, CA: Center for Geotechnical Modeling, Univ. of California Davis.
Mayne, P. W., and G. J. Rix. 1995. "Correlations between shear wave velocity and cone tip resistance in natural clays." *Soils Found.* 35 (2): 107–110. https://doi.org/10.3208/sandf1972.35.2_107.
McKenna, F., M. H. Scott, and G. L. Fenves. 2010. "Nonlinear finite-element analysis software architecture using object composition." *J. Comput. Civ. Eng.* 24 (1): 95–107. https://doi.org/10.1061/(ASCE)CP.1943-5487.0000002.
Mele, L., A. Chiaradonna, S. Lirer, and A. Flora. 2021. "A robust empirical model to estimate earthquake-induced excess pore water pressure in saturated and non-saturated soils." *Bull. Earthquake Eng.* 19 (Aug): 3865–3893. https://doi.org/10.1007/s10518-020-00970-5.
Mosher, R. L. 1984. *Load-transfer criteria for numerical analysis of axially loaded piles in sand*. Rep. No. K-84. Vicksburg, MS: US Army Engineer Waterways Experiment Station.
Olson, S. M., X. Mei, and Y. M. A. Hashash. 2020. "Nonlinear site response analysis with pore-water pressure generation for liquefaction triggering evaluation." *J. Geotech. Geoenviron. Eng.* 146 (2): 04019128. https://doi.org/10.1061/(ASCE)GT.1943-5606.0002191.
Petek, K., R. Mitchell, and H. Ellis. 2016. *FHWA deep foundation load test database version 2.0 user manual*. Rep. No. FHWA-HRT-17-034. McLean, VA: Federal Highway Administration.
Reese, L. C., and M. W. O'Neil. 1987. *Drilled shafts: Construction procedures and design methods*. Rep. No. FHWA-IF-99-025. McLean, VA: Federal Highway Administration.
Robertson, P. K. 2015. "Comparing CPT and V_s liquefaction triggering methods." *J. Geotech. Geoenviron. Eng.* 141 (9): 04015037. https://doi.org/10.1061/(ASCE)GT.1943-5606.0001338.
Seed, H. B., and I. M. Idriss. 1970. *Soil moduli and damping factors for dynamic response analyses*. Berkeley, CA: Earthquake Engineering Research Center, Univ. of California, Berkeley.
Seed, H. B., P. P. Martin, and J. Lysmer. 1976. "Pore-water pressure changes during soil liquefaction." *J. Geotech. Eng. Div.* 102 (4): 323–346. https://doi.org/10.1061/AJGEB6.0000258.
Shamoto, Y., J. Zhang, and K. Tokimatsu. 1998. "Methods for evaluating residual post-liquefaction ground settlement and horizontal displacement." *Soils Found.* 38 (Sep): 69–83. https://doi.org/10.3208/sandf.38.Special_69.
Sinha, S. K. 2022. "Liquefaction-induced downdrag on piles: Centrifuge and numerical modeling, and design procedures." Ph.D. dissertation, Dept. of Civil and Environmental Engineering, Univ. of California, Davis.
Sinha, S. K., K. Ziotopoulou, and B. L. Kutter. 2019. "Parametric study of liquefaction induced downdrag on axially loaded piles." In *Proc., 7th Int. Conf. on Earthquake Geotechnical Engineering*. London: International Society for Soil Mechanics and Geotechnical Engineering.
Sinha, S. K., K. Ziotopoulou, and B. L. Kutter. 2021a. "SKS02: Centrifuge test of liquefaction-induced downdrag in uniform liquefiable deposit." In *Centrifuge testing of liquefaction-induced downdrag on axially loaded piles*. Seattle: DesignSafe-CI. https://doi.org/10.17603/ds2-d25m-gg48.
Sinha, S. K., K. Ziotopoulou, and B. L. Kutter. 2021b. "SKS03: Centrifuge test of liquefaction-induced downdrag in interbedded soil deposits." In *Centrifuge testing of liquefaction-induced downdrag on axially loaded piles*. Seattle: DesignSafe-CI. https://doi.org/10.17603/ds2-wjgx-tb78.
Sinha, S. K., K. Ziotopoulou, and B. L. Kutter. 2022a. "Centrifuge model tests of liquefaction-induced downdrag on piles." In *Proc., 20th Int. Conf. on Soil Mechanics and Geotechnical Engineering*. London: International Society for Soil Mechanics and Geotechnical Engineering.
Sinha, S. K., K. Ziotopoulou, and B. L. Kutter. 2022b. "Centrifuge model tests of liquefaction-induced downdrag on piles in uniform liquefiable deposits." *J. Geotech. Geoenviron. Eng.* 148 (7): 04022048. https://doi.org/10.1061/(ASCE)GT.1943-5606.0002817.
Sinha, S. K., K. Ziotopoulou, and B. L. Kutter. 2022c. "Numerical modeling of liquefaction-induced downdrag: Validation against centrifuge model tests." *J. Geotech. Geoenviron. Eng.* 148 (12): 04022111. https://doi.org/10.1061/(ASCE)GT.1943-5606.0002930.
Sinha, S. K., K. Ziotopoulou, and B. L. Kutter. 2023. "Effects of excess pore pressure redistribution on liquefiable and non-liquefiable layers." *J. Geotech. Geoenviron. Eng.*
Stringer, M. E., and S. P. G. Madabhushi. 2013a. "Axial load transfer in liquefiable soils for free-standing piles." *Géotechnique* 63 (5): 400–409. https://doi.org/10.1680/geot.11.P.078.
Stringer, M. E., and S. P. G. Madabhushi. 2013b. "Re-mobilization of pile shaft friction after an earthquake." *Can. Geotech. J.* 50 (9): 979–988. https://doi.org/10.1139/cgj-2012-0261.
Sun, T. K., and W. M. Yan. 2010. "Development of neutral plane on a pile in a consolidating ground." *AIP Conf. Proc.* 1233 (1): 1594–1599. https://doi.org/10.1063/1.3452147.
Tokimatsu, K., and H. B. Seed. 1984. *Simplified procedures for the evaluation of settlements in clean sands*. Rep. No. NSF/CEE-84027. Berkeley, CA: Earthquake Engineering Research Center, Univ. of California Berkeley.
Vijivergiya, V. N. 1977. "Load-movement characteristics of piles." In Vol. 2 of *Proc., 4th Symp. of Waterway, Port, Coastal and Ocean Division*, 269–284. New York: ASCE.
Vucetic, M., and R. Dobry. 1991. "Effect of soil plasticity on cyclic response." *J. Geotech. Geoenviron. Eng.* 117 (1): 89–107. https://doi.org/10.1061/(ASCE)0733-9410(1991)117:1(89).
Wang, R., and S. J. Brandenberg. 2013. "Beam on nonlinear Winkler foundation and modified neutral plane solution for calculating downdrag settlement." *J. Geotech. Geoenviron. Eng.* 139 (9): 1433–1442. https://doi.org/10.1061/(ASCE)GT.1943-5606.0000888.
Wang, R., S. J. Brandenberg, and J. Zhang. 2015. "Calculation method of axial force and settlement of pile foundation during foundation consolidation and reconsolidation." *Chin. J. Geotech. Eng.* 37 (3): 512–518. https://doi.org/10.11779/CJGE201503015.
Wang, S., X. Lei, Q. Meng, J. Xu, M. Wang, and W. Guo. 2021. "Model tests of single pile vertical cyclic loading in calcareous sand." *Mar. Georesour. Geotechnol.* 39 (6): 670–681. https://doi.org/10.1080/1064119X.2020.1744048.
Wu, J. 2002. "Liquefaction Triggering and post-Liquefaction deformation of Monterey 0/30 sand under unidirectional cyclic simple shear loading." Ph.D. dissertation, Dept. of Civil and Environmental Engineering, Univ. of California, Berkeley.
Yoshimi, Y., and F. Kuwabara. 1973. "Effect of subsurface liquefaction on the strength of surface soil." *Soils Found.* 13 (2): 67–81. https://doi.org/10.3208/sandf1972.13.2_67.
Youd, T. L., et al. 2001. "Liquefaction resistance of soils: Summary report from the 1996 NCEER and 1998 NCEER/NSF workshops on evaluation of liquefaction resistance of soils." *J. Geotech. Geoenviron. Eng.* 127 (10): 817–833. https://doi.org/10.1061/(ASCE)1090-0241(2001)127:10(817).
Ziotopoulou, K., S. K. Sinha, and B. L. Kutter. 2022. "Liquefaction-induced downdrag on piles: Insights from a centrifuge and numerical modeling program." In *Proc., 4th Int. Conf. on Performance Based Design in Earthquake Geotechnical Engineering*. London: International Society of Soil Mechanics and Geotechnical Engineering.
Khosravi, M., J. T. DeJong, R. W. Boulanger, A. Khosravi, M. Hajialilue-Bonab, S. K. Sinha, and D. Wilson. 2022. "Centrifuge tests of cone-penetration test of layered soil." *J. Geotech. Geoenviron. Eng.* 148 (4): 04022002. https://doi.org/10.1061/(ASCE)GT.1943-5606.0002716.